Journal of Robotics and Control (JRC)
Volume 5, Issue 6, 2024
ISSN: 2715-5072, DOI: 10.18196/jrc.v5i6.23158 

# Design and Analysis of a Hybrid Intelligent SCARA Robot Controller Based on a Virtual Reality Model

Yousif Al Mashhadany [1*], Ahmed K. Abbas [2], Sameer Algburi [3], Bakr Ahmed Taha [4]
[1] Department of Electrical Engineering, College of Engineering, University of Anbar, Iraq
[2] University Headquarters, University of Anbar, Iraq
[3] Al-Kitab University, College of Engineering Technology, Iraq
[4] UKM, Photonics Technology Laboratory, Department of Electrical, Electronic
Email: [1] yousif.mohammed@uoanbar.edu.iq, [2] ahmed89at@uoanbar.edu.iq, [3] sameer.algburi@uoalkitab.edu.iq,
[4] bakerkufu955@gmail.com
*Corresponding Author

***Abstract*—SCARA robots have been used in various fields of robotics, such as biomedical engineering, automation, industrial, and gaming. However, our SCARA (Selective Compliance Assembly Robot Arm) VR model stands out with its realistic design and construction assumptions. The VR testing of the robot's motion envelope has facilitated a more precise inverse kinematics solution and verification of the dynamic process. The intelligent controller of this application, based on the Adaptive Neuro-Fuzzy Inference System (ANFIS) technique and a classical proportional-integral-derivative (PID) controller, offers an optimized solution to the accuracy problem. The hybrid ANFIS controller starts with the PID setting parameters of the resultant solution. Following thorough testing of the suggested SCARA manipulator with an intelligent controller in a virtual reality environment, researchers recognized the physical system's potential for implementation utilizing multiple control approaches. Despite the intricacy of its design and implementation, the intelligent controller's software ensures that the system runs at top efficiency. This application replicates the user interface of the MATLAB/SIMULINK var (2022b), which produced promising robotics results, demonstrating its trustworthiness as a realistic, intelligent model, and virtual reality was critical in the development of the SCARA manipulator. It digs into the design and analysis of a hybrid intelligent controller for SCARA robots, which are widely used in assembly lines and manufacturing. Finally, the proposed controller combines the best features of an Adaptive Neuro-Fuzzy Inference System (ANFIS) with a conventional proportional-integral-derivative (PID) controller to resolve application accuracy difficulties as efficiently as possible.**

***Keywords—SCARA Manipulator; Inverse Kinematic Solution; Hybrid Intelligent Controller; Virtual Reality; ANFIS Methodology.***

## I. INTRODUCTION

Designing and analyzing a SCARA robot hybrid intelligent controller based on a virtual reality model is a challenging and multidisciplinary approach. Integrating SCARA robots with virtual reality and hybrid intelligent controllers requires a better understanding of robotics, control systems, and virtual reality technology [1][2]. For decades, many studies have focused on the development of manufacturing robots, which are widely utilized in numerous applications, particularly in mechanical work, aerospace, defense, decision making and operations, painting, and soldering [3][4]. Furthermore, the robot is employed in medical procedures like as surgery, where the location of the end effector (position of a robotic) is critical to achieving improved accuracy [5]-[7]. They are employed to assist the human administrator during the activity, so improving exhibition and precision, as well as the robot control system's strength in transportation, medical, and modern settings. They can also be employed instead of humans in high-risk situations, such as a radioactive site. Thus, the robot is used to aid the human administrator increase the preciseness and accuracy of the action [8]-[12].

Selective Compliance Articulated Robot Arm (SCARA) with three revolute joints and one prismatic (degrees of freedom, DOF) became standard in production systems in the factory and used in assembly lines and packaging. This type of automaton was initially introduced by (Hiroshi Makino) [13][14]. Today, modern (SCARA) robots are created with numerous sizes, weights, and linear speeds. Currently, industrial applications use intelligent control systems for robots [15]. SCARA controllers frequently execute tasks such as deformity removal, pick-spot, brushed gap pegging, circuit board assembly, and mechanical assembly, all of which need precise tracking and rapid movement within the end-effector. Traditional high-speed robots cannot handle enormous weights (10-20 kg), while robots carrying massive payloads cannot travel at high speeds. The servo motors allow for rapid speeds and payloads. Higher speeds are frequently achieved utilizing parallel kinematic devices with actuators [16]-[20], as illustrated in Fig. 1. Researchers have reached rising velocities of up to 785 ms2, which is around 80% of the rate of gravitational acceleration. To address the inactivity issue, belt drives divide the drive system segments by numbering the power transmission and actuator segments from the emotional parts. This is because, as it may, the system becomes acquainted with the backfire and erosion [21][27].

A few studies have proposed alternatives, such as the wire-driven fast-load conveyance (FALCON) robot. Degrees of freedom (3-DOF) Mini Cheetah robots (MIT's) Toumi and Kuo envisioned a direct-drive regulator. The velocity reached 3 m/s, which indicates that it may accelerate up to 3.8 times the gravitational velocity (precisely between 0.05 mm as well as 0.1 mm). There has been no investigation into a hydraulic solution for the high-speed, high-payload problem [28][35].

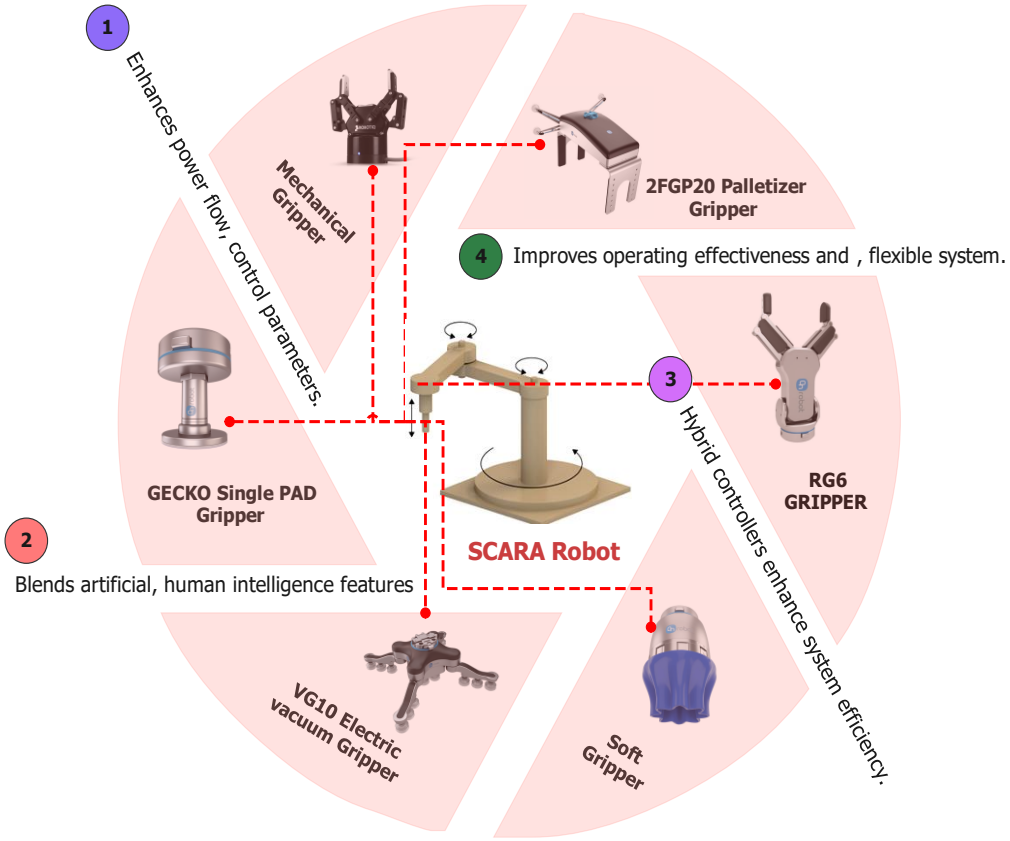


Fig. 1. Illustrates the features of a SCARA robot and many robotic grippers, intelligence, control, and system efficiency improvements

Vibration can also be an issue in planar operations, which frequently use SCARA controls. Brushless DC motors, which can generate extremely large torques but also increase system inertia, are typically used to guide traditional inexpensive SCARA controllers. Beating the issue of revolute joints connected by belt or gear drives, notwithstanding the presence of postponed friction and slip [36]-[40]. At extremely high speeds, the massive payload of an electric motor-driven SCARA is impossible. The research into servo-hydraulic component technology was limited to high-torque force applications. There are a few servo-hydraulic actuators that are suited for controlling sequential devices. Various linear actuators have been used to power revolving joints, vary torque across the operating range, and limit execution. Studies on turning actuators have not yet been undertaken. Other studies have considered rotational actuators for high-torque utilization. None earlier have utilized servo-hydraulics power to create high speeds in serial controllers (manipulators serial) [41][42].

Designed an economical SCARA robot has been done based on a conventional PID controller. Deciding Denavit-Hartenberg (DH) specifications is the initial step for inferring robots' mechanics (kinematics). The arranged method was connected to the robot, as indicated by the DH. The SCARA robot offers great execution, for example, (~±0.01 mm repeatability), a peak linear speed of (8.5 m/s) in x-y, (0.5 s) the time of pick and spot process duration, and an adaptable control system. The results demonstrated a low error during the quick trajectory. The trajectory is tracked with great accuracy in (the position and speed). A limited component analysis was used to decrease the total weight of the robot links [43]-[47]. Based on the mechanics (kinematics) principle, an inverse kinematics analysis algorithm for the (two degrees of freedom) SCARA mechanism is derived, which is tested and confirmed using the PMAC multi-axis motion controller. Analytical calculations can be used to successfully understand the inverse kinematics solution of the robot mechanism, and the user can accomplish the corresponding track motion by programming the mechanism end actuator assortment position [48][49].

Moreover, in the investigation of the simulation which has been used, (4-DOF) SCARA robot (Selective Compliance Assembly, with three moves of joints and one prismatic joint to appreciate handling. The structure was constructed using (CAD) software. Controller technology leads to automated movement. The product has been completed based on efficiency increase, quality development together with less aberration, timely delivery, limited maintenance, and more safety aspects (Table II). shows the uses of robots and a comparison of the types of control, accuracy, etc. [50]-[54]. Modeling of a (4-DOF) SCARA robot system (axes) using the Denavit-Hartenberg formula and kinematic equalization of the SCARA robot. Mechanism Characteristics: The extensive investigation used DC servomotors for each of the robot's arm joints. A four-axis SCARA system was integrated using the virtual reality modelling language (VRML). The SCARA robot was simulated using MATLAB/Simulink tool package software. The design is based on (solid-body) design and VR technology. The reaction was swift, and time utilization was possible using interface cards [55][56].

## II. RESEARCH IN CONTEXT

### A. Evidence Before this Study

Robot-assisted training (RAT) is acknowledged for improving efficiency and accuracy in many applications within biomedical engineering, automation, industrial sectors, and gaming. The SCARA robot arm is highly adaptable because it directly addresses kinematic and dynamic obstacles.

### B. Problem Statement

Integrating sensors into SCARA robotic end effectors presents several challenging issues that, if resolved, would enable a system that is both efficient and resilient, and performs accurately under regulated settings. The data collected by the sensors allows the robot to perform activities such as placement, assembly, and selection of parts, but additional difficulties arise when modifying the end effector for various materials and settings. To be effective, the system must be able to adjust its strength, shape, and size to accommodate a wide range of weights, sizes, and shapes, and be capable of operating safely and effectively in various environments such as high and low temperatures, high and low humidity, and small spaces. The ability of a sensor system to identify and respond to possible collisions is crucial for reducing the likelihood of harm to the robot and its environment. Overcoming the challenges related to security, performance, scalability, and detection accuracy is essential for creating a system in which SCARA robots can rely on and adapt to perform better in industries such as automation, assembly, and manufacturing. This study focuses on the problem of robotic end-effectors equipped with sensors, with the aim of developing a system that addresses these challenges and enhances the performance of SCARA robots, because one of the most important problems of factories in production lines is the accuracy of the sensors used, supported by artificial intelligence software, to identify and distinguish between a good product and a defective product, as well as the need for some industrial applications. To distinguish between products according to the efficiency of performance and divide them according to the degree of efficiency into different groups, as happens in the examination and differentiation of solar cells. The study will also seek to implement a simulation of an integrated industrial system to find an appropriate solution between the speed required in isolating the bad product and its keeping pace with the required production speed, on the basis of which it is evaluated. Factory performance.

## III. MATHEMATICAL MODELING OF THE ROBOT

Kinematics are divided into two types: inverse kinematics and forward kinematics. In inverse kinematics (IK), the length of every connection and the position of the objective inside the work volume are given, and we need to determine the angle of every joint. In forward kinematics (FK), the length of every connection and subsequently the angle of every connected join are given, and we must find the position of any function within the work volume. In kinematic analysis, the positions and speeds of all joint connections were determined [57]–[61].

### A. Inverse Kinematics Modeling

Inverse Kinematic model discovers more potential utilization in practical systems. The Inverse Kinematic model measures the joint angles required to achieve the given position and orientation. The IK model finds important things in other fields such as 3D games. In contrast to forward kinematics, the solutions that ensure collision-free operation and the least possible joint motion are studied more optimally [62][63], see Table I.

TABLE I. LISTS THE DH PARAMETERS OF THE ROBOT ARM

| J | Dj | θj | Aj | αj |
|---|---|---|---|---|
| 01 | 0.0 | $\theta_1$ | $A_1$ | 0.0 |
| 02 | 0.0 | $\theta_2$ | $A_2$ | 0.0 |
| 03 | $D_3$ | 0 | 0 | 0.0 |
| 04 | $D_4$ | $\theta_4$ | 0 | 0.0 |

According to Table I [11], we can write the transformation matrices as

$$T_1^0 = F_1 = \begin{bmatrix} c\theta_1 & s\theta_1 & 0 & A_1 \\ -s\theta_1 & c\theta_1 & 0 & A_1 c\theta_1 \\ 0 & 0 & 1 & 0 \\ 0 & 0 & 0 & 1 \end{bmatrix} \quad (1)$$

$$T_2^1 = F_2 = \begin{bmatrix} c\theta_2 & s\theta_2 & 0 & A_2 s\theta_2 \\ -s\theta_2 & c\theta_2 & 0 & A_2 c\theta_2 \\ 0 & 0 & 1 & 0 \\ 0 & 0 & 0 & 1 \end{bmatrix} \quad (2)$$

$$T_3^2 = B_3 = \begin{bmatrix} 1 & 0 & 0 & 0 \\ 0 & 1 & 0 & 0 \\ 0 & 0 & 1 & -D_3 \\ 0 & 0 & 0 & 1 \end{bmatrix} \quad (3)$$

$$T_3^2 = B_3 = \begin{bmatrix} c\theta_4 & s\theta_4 & 0 & 0 \\ -s\theta_4 & c\theta_4 & 0 & 0 \\ 0 & 0 & 1 & -D_4 \\ 0 & 0 & 0 & 1 \end{bmatrix} \quad (4)$$

The overall transformation matrix can be expressed as

$$T_4^0 = \begin{bmatrix} c\theta_1 c\theta_2 c\theta_4 & s\theta_1 s\theta_2 s\theta_4 & 0 & A_2 s\theta_1 + A_1 s\theta_1 \\ -s\theta_1 s\theta_2 s\theta_4 & c\theta_1 c\theta_2 c\theta_4 & 0 & A_2 c\theta_1 c\theta_2 + A_1 c\theta_1 \\ 0 & 0 & 1 & -D_3 - D_4 \\ 0 & 0 & 0 & 1 \end{bmatrix} \quad (5)$$

#### 1) Position inverse calculation

The desired location matrix of the SCARA robot can be written as

$$T_H^R = \begin{bmatrix} N_x & O_x & A_x & P_x \\ N_y & O_y & A_y & P_y \\ N_z & O_z & A_z & P_z \\ 0 & 0 & 0 & 1 \end{bmatrix} \quad (6)$$

The overall transformation matrix of the robot can be considered an equivalent matrix of the desired location, as follows [26]:

$$T_H^R = F_1 F_2 F_3 F_4 = T_4^o \quad (7)$$

The calculation of F4 can be performed using Eq. (1) to Eq. (4) and Eq. (6) then substituted by Eq. (7), we obtain:

$$F_3^{-1} F_2^{-1} F_1^{-1} T_H^R = F_4 \quad (8)$$

$$\begin{bmatrix} N_x c\theta_1 c\theta_2 + N_y s\theta_1 s\theta_2 & O_x c\theta_1 c\theta_2 + O_y s\theta_1 s\theta_2 & A_x c\theta_1 c\theta_2 + A_y s\theta_1 s\theta_2 & P_x C\theta_1 C\theta_2 + P_y s\theta_1 s\theta_2 - A_1 s\theta_2 - A_2 \\ -N_x s\theta_1 s\theta_2 + N_y c\theta_1 c\theta_2 & O_x s\theta_1 s\theta_2 + O_y c\theta_1 c\theta_2 & -A_x s\theta_1 s\theta_2 + A_y c\theta_1 c\theta_2 & -P_x s\theta_1 s\theta_2 + P_y c\theta_1 c\theta_2 - A_1 s\theta_2 \\ N_z & O_z & A_z & P_z + D_3 \\ 0 & 0 & 0 & 1 \end{bmatrix} = F_4$$

TABLE II. SHOWS THE USE OF ROBOTS AND A COMPARISON OF THE TYPE OF CONTROL, ACCURACY, ETC

| Ref. | Application | Type Of Controller | Type Of Gripper | Accuracy | Implement or Simulation |
|---|---|---|---|---|---|
| [49] | Arm Manipulator 6 DOF robotic arm | (ED-Mark IV) is | rubber pads | precision of ±0.5cm | Simulation |
| [50] | Industrial Application | (ANFIS) (FLC) | rotation signal of the SCARA joints and translation of the gripper movements | The method is effective, and the response (settling) is fast. | Simulation |
| [30] | Surgical skin cutting | A PID controller & PI/Feedforward controller | 4 Degrees of Freedom (DOF) Selective Compliance Articulated Robot Arm | simulated with success. | Simulation |
| [51] | 3D printers | Differential-Algebraic Equations (DAE) | four arms SCARA (Selective Compliance Articulated Robot for Assembly) | increasing the supply voltage. | Simulation |
| [48] | scenarios of industrial robots. | The software includes RC+ 7.0 robot control software, Unity3D engine and Visual Studio 2013 development tools | industrial robots based on Virtual Reality technology | the result shows that the system has obtained the real-time control objective, | Implement and Simulation |
| [52] | Human-Link Manipulator | (ANFIS)& (NN) | 7-DOF | Palatable outcomes are implemented | Simulation |
| [53] | RPP robot | fuzzy PD controller | RPP robot has three degrees of freedom | better controlling performance in comparison with other controllers. | Simulation |
| [54] | industrial manipulator that shares its workspace with humans | controller CR751–D. | four DOF industrial | more-effective | Simulation |
| [55] | position tracking for SCARA robot | PCH and backstepping | 2-DOF | good dynamic performance, good steady-state performance and strong resistance to external interference. | Simulation |
| [42] | trajectory tracking of robot | DTSMNAC | 2 DOF | hows to be able to ensure that the output tracking error will converge to zero | Simulation |
| [56] | control the joint-angle position of the SCARA parallel robot | neural controller and PID controller | 2 DOF | reduce the tracking error to nearly zero | Implement and Simulation |
| [44] | in order to address the kinematic analysis | (FIS) and (NNA). | 4-DOFs | It has been demonstrated with simulation runs that results are satisfactory | Simulation |
| [57] | SCARA robot | PID | 2 DOF | show the increasing of performance and stability. | Simulation |
| [58] | Trajectory Tracking | fuzzy-PI | 3 DOF | improved performance characteristics in terms of highly reduced maximum absolute error. | Simulation |
| [59] | trajectory planning, | PID | 2 DOF | This model provides an open-source platform for robot trajectory planning and motion control algorithms. | Simulation |
| [60] | trajectory planning | Arduino and OpenCM9.04 control cards | 5 DOF | very successful results were achieved. | Simulation |

Based on the compression of Eqs. (4) and Eq. (8), it can be concluded that Eq. (9) and (10) as:

$$P_x = A_2 s\theta_1 + A_2 s\theta_1 s\theta_2 \quad (9)$$

$$P_y = A_2 c\theta_1 + A_2 c\theta_1 c\theta_2 \quad (10)$$

Same as with Eq. (9) and Eq. (10) yields the following:

$$s\theta_2 = \frac{1}{2A_1A_2}(P_x^2 + P_x^2 - A_1^2 - A_2^2) \quad (11)$$

$$c\theta_2 = \pm\sqrt{1 - (s\theta_2)^2} \quad (12)$$

$$\theta_2 = tan^{-1}\frac{c\theta_2}{s\theta_2} \quad (13)$$

Eq. (9) and Eq. (10) can be rewritten as

$$P_x = (A_1 + A_2 s\theta_2)s\theta_1 - A_2 c\theta_2 c\theta_1 \quad (14)$$

$$P_y = A_2 c\theta_2 c\theta_1 + (A_1 + A_2 s\theta_2)c\theta_1 \quad (15)$$

The solving Eq's. (14)(15) can be performed using Kramer's formula, as follows:

$$\Delta = \begin{bmatrix} A_1 + A_2 s\theta_2 & -A_2 c\theta_2 \\ A_2 c\theta_2 & A_1 + A_2 s\theta_2 \end{bmatrix} = (A_1 + A_2 s\theta_2)^2 + (A_2 c\theta_2)^2 \quad (16)$$

$$\Delta s\theta_1 = \begin{bmatrix} A_1 + A_2 s\theta_2 & -P_x \\ A_2 c\theta_2 & -P_y \end{bmatrix} = (A_1 + A_2 s\theta_2)P_x + (A_2 c\theta_2)P_y \quad (17)$$

$$\Delta c\theta_1 = \begin{bmatrix} P_x & -A_2 c\theta_2 \\ P_y & -A_1 + A_2 s\theta_2 \end{bmatrix} = (A_1 + A_2 s\theta_2)P_y + (A_2 c\theta_2)P_y \quad (18)$$

$$c\theta_1 = \frac{\Delta c\theta_1}{\Delta} = \frac{(A_1 + A_2 s\theta_2)P_x - A_2 c\theta_2 P_x}{(A_1 + A_2 s\theta_2)^2 + (A_2 c\theta_2)^2} = \frac{(A_1 + A_2 s\theta_2)P_y - A_2 c\theta_2 P_y}{(P_x)^2 + (P_y)^2} \quad (19)$$

$$s\theta_1 = \frac{\Delta s\theta_1}{\Delta} = \frac{(A_1+A_2s\theta_2)P_x - A_2c\theta_2P_x}{(A_1+A_2s\theta_2)^2+(A_2c\theta_2)^2} = \frac{\frac{(A_1+A_2s\theta_2)P_x - A_2c\theta_2P_y}{(P_x)^2+(P_y)^2}}{} \quad (20)$$

$$\theta_1 = tan^{-1}\frac{s\theta_1}{c\theta_1} = tan^{-1}\frac{(A_1+A_2s\theta_2)P_y - A_2c\theta_2P_x}{(A_1+A_2s\theta_2)P_x - A_2c_{\theta 2}P_y} \quad (21)$$

According to the comparison between cell (4, 4) in the matrix for Eq. (5) and Eq. (6) will get:

$$D_3 = -P_z - D_4 \quad (22)$$

$$\theta_1 = 0 \quad (23)$$

According to the comparison between cells (1, 1) in the matrix for Eq. (4) and (2, 1) in the matrix of Eq. (8) will get:

$$s\theta_4 = N_x s\theta_1 s\theta_2 + N_y s\theta_1 s\theta_2 \quad (24)$$

$$c\theta_4 = -N_x s\theta_1 s\theta_2 + N_y s\theta_1 s\theta_2 \quad (25)$$

$$\theta_4 = tan^{-1}\frac{-N_y sin(\theta_1+\theta_2)+N_y cos(\theta_1+\theta_2)}{N_x cos(\theta_1+\theta_2)+N_y sin(\theta_1+\theta_2)} \quad (26)$$

*2) Velocity inverse calculation*

Based on the inverse solution of Eq. (9) and Eq. (10) yields the following:

$$\dot{P}_x = -A_1c\theta_1\dot{\theta}_1 - A_2c\theta_1c\theta_2\left(\dot{\theta}_1+\dot{\theta}_2\right) \quad (27)$$

$$\dot{p}_x = -A_1c\theta_1\dot{\theta}_1 - A_2c\theta_1c\theta_2\left(\dot{\theta}_1+\dot{\theta}_2\right) \quad (28)$$

By rearrange:

$$\dot{p}_x = -(A_1c\theta_1+A_1)\dot{\theta}_1 - A_2c\theta_1c\theta_2\dot{\theta}_2 \quad (29)$$

$$\dot{p}_y = -(A_1s\theta_1+A_2c\theta_1c\theta_2)\dot{\theta}_1 + A_2c\theta_1c\theta_2\dot{\theta}_2 \quad (30)$$

Based on the solution to Eq. (29) and Eq. (30) using Kramer's formula, as follows:

$$\dot{\theta}_1 = \frac{\dot{P}_x s\theta_1 s\theta_2 + \dot{p}_y c\theta_1 c\theta_2}{A_1 c\theta_2} \quad (31)$$

$$\dot{\theta}_2 = \frac{-\dot{p}_y(A_1c_1+A_2c\theta_1c\theta_2) - -\dot{p}_x(A_1s\theta_1+A_2s\theta_1s\theta_2)}{A_1A_2c\theta_2} \quad (32)$$

The Translational velocity form is:

$$\dot{D}_2 = -\dot{P}_z \quad (33)$$

By differentiating Eqs. (26) as:

$$s\theta_4 d\theta_4 = -[dN_x c\theta_1c\theta_2(d\theta_1+d\theta_2)] + d_{ny}s\theta_1s\theta_2 - N_y c\theta_1c\theta_2(d\theta_1+d\theta_2) \quad (34)$$

So,

$$d\theta_4 = -\frac{d\theta_1+d\theta_2}{s\theta_4}\left(n_x s\theta_1s\theta_2 + n_y c\theta_1c\theta_2\right) - \frac{c\theta_1c\theta_2}{s\theta_4}dN_x + \frac{s\theta_1s\theta_2}{s\theta_4}dN_y \quad (35)$$

$$\dot{\theta}_4 = \frac{d\theta}{dt} = \frac{s\theta_1s\theta_2\dot{N} - c\theta_1c\theta_2\dot{N}_x - \left(N_x s\theta_1s\theta_2 + N_y c\theta_1c\theta_2\right)\dot{\theta}_{12}}{s\theta_4} \quad (36)$$

*3) Acceleration inverse calculation*

$$\ddot{\theta}_1 = \frac{-\left(\dot{p}_x c\theta_1c\theta_2 + \dot{p}_y s\theta_1s\theta_2\right)\dot{\theta}_{12} + \left(\ddot{p}_x s\theta_1s\theta_2 + \ddot{p}_y c\theta_1c\theta_2\right) - A_1s\theta_2\dot{\theta}_1\dot{\theta}_2}{A_1c\theta_1} \quad (37)$$

$$\ddot{\theta}_2 = \frac{\left[(\ddot{p}_x c\theta_1 - \ddot{p}_x s\theta_1)A_1 + (\ddot{p}_x c\theta_1c\theta_2 - \ddot{p}_x s\theta_1s\theta_2)A_2 + \left(\dot{p}_y s\theta_1 - \dot{p}_x c\theta_1\right)A_1\dot{\theta}_1 + \left(\dot{p}_y s\theta_1s\theta_2 + \dot{p}_x c\theta_1c\theta_2\right)A_2\dot{\theta}_{12} + A_1A_2\left(\dot{\theta}_2\right)^2\right]}{A_1A_2c\theta_2} \quad (38)$$

$$\ddot{d}_3 = -\ddot{p}_x \quad (39)$$

$$\ddot{\theta}_4 = \frac{\ddot{N}_y s\theta_1s\theta_2 - \ddot{n}_x c\theta_1c\theta_2 - \left(2\dot{N}_y c\theta_1c\theta_2 + 2\dot{N}_x s\theta_1s\theta_2\right)\ddot{\theta}_{12} - \left(N_y s\theta_1s\theta_2 - N_x c\theta_1c\theta_2\right)\left(\dot{\theta}_{12}\right)^2 - \left(N_x s\theta_1s\theta_2 + N_y c\theta_1c\theta_2\right)\ddot{\theta}_{12} + c\theta_4\left(\dot{\theta}_4\right)^2}{s\theta_4} \quad (40)$$

*B. Dynamics Formulation of the Robot*

The torques of every joint in the robot presented in Fig. 2 can be expressed as [64]:

$$T_1 = f_{11}\ddot{\theta}_1 - f_{12}\ddot{\theta}_1 - f_{13}D_3 - f_{14}\dot{\theta}_1\dot{\theta}_2 + f_{15}\left(\dot{\theta}_2\right)^2 \quad (41)$$

$$T_2 = f_{21}\ddot{\theta}_1 + f_{22}\ddot{\theta}_2 + f_{23}\ddot{D}_3 + f_{24}\left(\dot{\theta}_2\right)^2 \quad (42)$$

$$T_3 = -f_{31}\ddot{\theta}_1 + f_{32}\ddot{\theta}_2 + f_{33}\ddot{D}_3 - f_{34} \quad (43)$$

By considering the following definitions of the parameters in Eq. (41)-(43):

$$f_{11} = (r_1)^2m_1 + i_1 + g_{r1}^2i_{m1} + ((A_1)^2 + (r_2)^2 + 2A_1r_2c_2)m_2 + (A_1)^2m_{m2} + i_2 + i_{m2} + \left((A_1)^2 + (A_2)^2 + 2A_1A_2c\theta_2\right)(m_3 + m_{m3}) + i_3 + i_{m3}$$

$$f_{12} = ((r_2)^2 + A_1r_2s_2)m_2 + i_2 + g_{r2}i_{m2} + ((A_1)^2 + A_1A_2s\theta_2)(m_3 + m_{m3}) + i_3 + i_{m2}$$

$$f_{13} = g_{r3}i_{m3};\ f_{14} = 2A_1c\theta_2[m_2r_2 + (m_3 + m_{m3})A_2]$$

$$f_{15} = A_1c\theta_2[m_2r_2 + (m_3 + m_{m3})A_2]\ ;\ f_{15} = A_1c\theta_2[m_2r_2 + (m_3 + m_{m3})A_2]$$

$$f_{21} = m_2((r_2)^2 + A_1r_2s_2) + i_2 + g_{r2}i_{m2} + ((A_1)^2 + A_1A_2s\theta_2)(m_3 + m_{m3}) + i_3 + i_{m3}$$

$$f_{22} = (r_2)^2m_2 + i_2 + g_{r2}^2i_{m2} + (A_2)^2(m_3 + m_{m3}) + i_3 + i_{m3}$$

$$f_{23} = g_{r3}i_{m3};\ f_{24} = A_1c\theta_2[m_2r_2(m_3 + m_{m3})A_2]$$

$$f_{31} = f_{32} = g_{r3}i_{m3}\ ;\ f_{33} = m_3 + g_{r3}i_{m3}\ ;\ f_{34} = m_3g$$

### C. Modeling of the Actuator

One of the most crucial parts of a robotic system is its actuator. The mechanism could be a computer that transforms energy into motion. There are various sorts of mechanisms, including hydraulic, pneumatic, mechanical, and electric. Most DC-servo motor engines are used in automated systems. An actuator is a machine that moves within an automaton. The machine types included cylinders (pneumatic and hydraulic) and motors. The elaborate actuator type is the Dc motor which will be derived for use throughout this analysis. To regulate the voltage and provide, the motor drive can use Pulse Width Modulation (PWM) control that uses microcontrollers for these benefits [65][66]:

- Light weight
- Small size
- Less the input and output
- The voltage of the armature can be variable with less loss.

By considering a constant flux, the model of the DC motor (separate-wound) at the permanent magnet can be expressed as (44)-(47) [67].

$$V_{a_1} = Ri_{a_1} + E_{a_1} + L\frac{di_{a_1}}{dt} \quad (44)$$

$$e_{a_1} = k_{\omega_1}\omega_{m_1} \quad (45)$$

$$T = k_{e_1}\varphi i_{a_1} = k_T i_{\omega_1} \quad (46)$$

$$T = T_{L_1} + j_{m_1}\frac{d\omega_m}{dt} + b\omega_{m_1} \quad (47)$$

### D. Transmission System Modeling

The robot design incorporates a variety of transmission components. The transmission is designed to transfer mechanical energy from the mechanism system to the load. The most crucial components of robots are the gears that are used for everyday transportation. Transmission is only allocated to the gearbox, which uses gears to convert speed and torque from a rotary motor shaft. Robots typically use a harmonic drive in their (revolute-joint) transmissions. The advantage of drives with parallel shafts is an unusually high-altitude transmission quantitative relationship in built-in bundles. The sender torque on the motor shaft (T) is often calculated using the following equation:

$$T = \frac{T_{L_1}}{g_r\eta} \Rightarrow T\frac{\omega_{m_1}}{\omega_{L_1}}\eta = T\frac{\theta_{m_1}}{\theta_{L_1}}\eta = T_{L_1} \quad (48)$$

$$J = j_{m_1} + \frac{J_{L_1}}{(g_r)^2} \quad (49)$$

The linear velocity of the third joint can be expressed as

$$\omega_{m_1} = \frac{D}{2} = \dot{D}_3 \quad (50)$$

## IV. METHODS AND MATERIALS

The proposed methodology involves the creation of a sophisticated robotic vision system capable of reliably identifying and manipulating objects, as illustrated in Fig. 2. Initially, we captured RGB images of the items and subsequently converted them to grayscale to facilitate the data processing. By employing Canny Edge Detection, we were able to determine the shapes of objects from the grayscale images. Real-time processing was performed on the collected data, which were continuously acquired. We conducted a thorough evaluation to determine whether we had obtained an adequate number of data points. Once a sufficient dataset was accumulated, a fitting algorithm was employed to generate a virtual curve, which was then stored in a database. The system utilizes this curve to mathematically model and recognize the edge of an item.

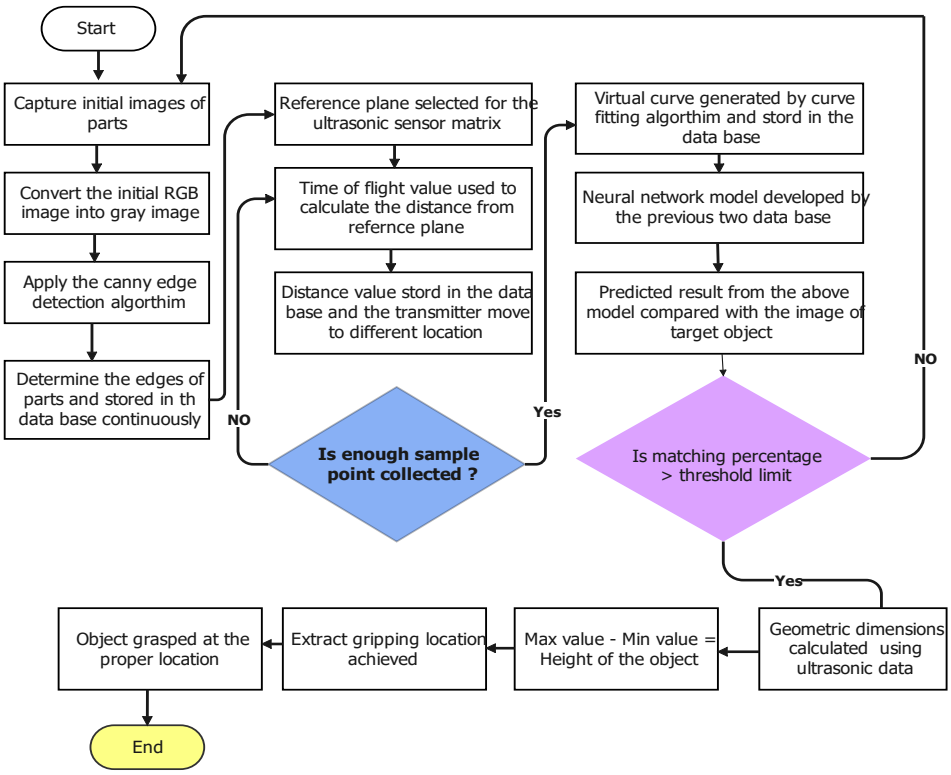


Fig. 2. Overall description of the proposed research methodology

Simultaneously, a Neural Network Model (NNM) was used to estimate the target object's properties from the recorded data. The ultrasonic sensor matrix chose a reference plane and used time-of-flight distance data to establish the object's exact location by providing essential depth information. The system then determines whether the neural network's prediction is close enough to the actual object to pass a specified accuracy test. After reaching the threshold, the robotic system moved on to the grabbing phase, where it used geometric measures derived from ultrasonic data to establish the precise placement and size of the item.

The system triggers the robotic arm to grasp the object at a specified position if the matching percentage is within the permissible range. This method holds great promise for use in robotics and industrial automation because it integrates edge detection, sample analysis, machine learning, and sensor technologies to achieve precise object manipulation

### *A. Sensor Classification in Spherical Coordinate-Based Articulated Robotic Arms*

The classification of sensors in spherical coordinate articulated robot arms is vital for designing and controlling robotic arms. Robotic arms can be equipped with a variety of sensors to increase their usefulness and performance. For example, a three-axial force sensor based on fiber Bragg gratings may detect external forces on a robotic arm from several degrees of freedom (DoF) using a single compact sensor. It offers a tiny and adjustable force measuring method for spherical coordinate articulated robot arms with flexible outer and robotic arms [38-40]. Vision-based sensing approaches for cyclic robotic arms have also been studied. Three actuators operated the spherical robotic arm and supplied sensory feedback for both rotating axes, one of which included a camera [41][42]. Vision-based sensors can provide complete feedback while controlling a spherical-coordinate articulated robot arm.

Furthermore, according to Yang et al. (2023), sensor fusion technology can improve the accuracy of anthropomorphic robotic arm control by merging the information from several sensors [43][44]. Thus, it is clear that achieving reliable and precise control of spherical coordinate articulated robot arms requires integration of several sensors. To further improve human-robot interactions, researchers have investigated the use of tactile sensors to provide robotic arms with the ability to perceive social touch [45]. Touch sensors are essential for spherically coordinated articulated robot arms to perform realistic movements and intuitive interactions. In conclusion, there is great promise for combining several types of sensors, such as tactile, vision-based, sensor fusion, and force sensors.

### *B. Components and Schematic Models of the System*

The robot's main goal is to identify, select, and operate the appropriate parts for assembly to complete the process of mating the parts to construct the finished goods with the aid of the applied embedded sensor. As depicted in Fig. 3. The F/T sensor used for this work met the following specifications: A six-axis force/torque sensor (Model No.: 9105-NET- GAMA - IP65) mounted on the SCARA robot's wrists and equipped with a suitable gripper detects the force and/or torque acting on the manipulation during a "obstacle encounter. To detect the presence or absence of a certain object, two proximity detection sensors, one capacitance (Model: CR30-15DP) and one inductive (Model: E2A-S08KS02-WP-B1-2M), were attached within the robot gripper. The proximity sensor used for this purpose meets the following criteria. The programmable logic controller (PLC) communicates with the sensor's ON/OFF signal outputs. Tactile and Ultrasonic Sensors (Light Touch Sensor Model: EVPAA and MA40S4R/S, respectively) were also positioned on the end-effector of the SCARA robot to detect the intended item's proximity to the end-effector and to signal the gripper's exerted force on the target item.

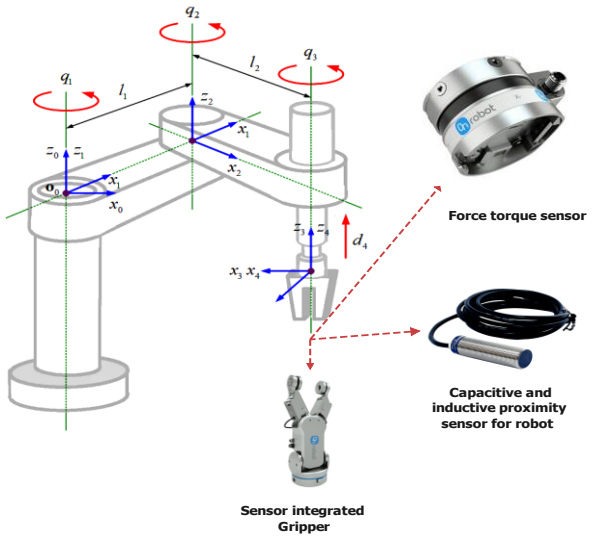


Fig. 3. SCARA robot configuration

### *C. Techniques for Interfacing and Collecting Data*

As shown in Fig. 2, the DAQ system connects the PC to the plan of the interface of all specified instruments with the SCARA robot, the F/T sensor, and the vision sensor. The information collection device transforms the voltages that are analogue to the sensor signals into digital values. The data were processed using MATLAB 2019a. By employing the ladder design and PLC software device, proximity detectors were interfaced and successfully controlled by programming a PLC. Similar to this, Fig. 2 shows how ultrasonic as well as tactile (LTS) sensors are connected using microcontrollers.

An intelligent robotic arm must have the ability to comprehend interactive information in unproductive surroundings, notably exterior data, such as distance, closeness, and force. Only a small percentage of the currently available industrial robotic end-effectors can fully sense both internal and exterior information, and the majority rely entirely on visual systems. A multisensory approach was used to perceive the necessary data for the automated operation. Several sensors were employed to gather data on items, industries, and the environment.

### *D. Distance and Position Detection Sensors*

To ensure accurate data collection, a combination of sensors is employed, including those for distance and location recognition, as well as a vision detector and ultrasound sensor. The latter is used to direct both the autonomous manipulation and the final effector in determining the 2D surface, position, distance, and form of each component in

the working area and to identify the object in question and its components. Specifically, a 40 KHz square pulse signal was transmitted by an ultrasonic distance sensor positioned in the area between both fingers whenever a 5V P-P square wave was applied to it, as illustrated in Fig. 4.

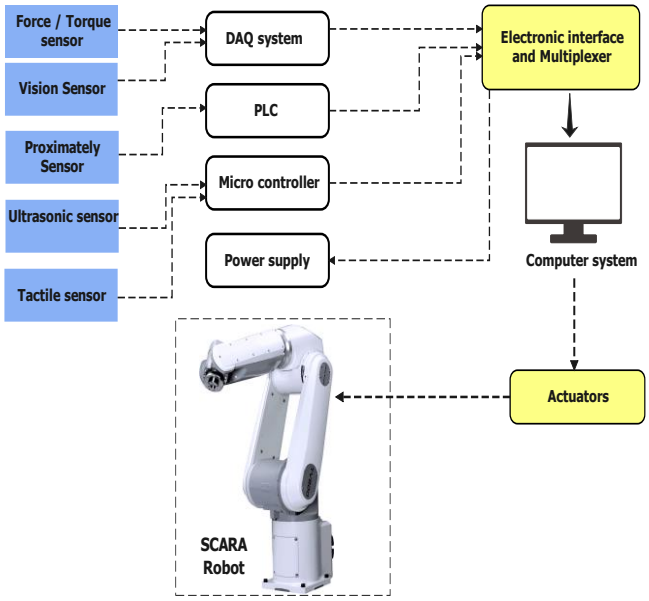


Fig. 4. Types of Sensors implemented with the SCARA robot

### *E. Hybrid Intelligent Controller Proposed Design*

There are two distinct techniques: Model Reference Adaptive Control (MRAC) and Direct Reference Adaptive Control (DRAC), both of which are very efficient and simple to construct a control following system performance through the use of previous system performance. They must address the difficulties of quantity optimization by limiting prices. They used data from previous trials to improve the reference input for the current trial, resulting in a hybrid (ANFIS) controller that is dependent on the model's classical controller; however, with the (ANFIS) reference input modification, the system's output is approximated from the required to the factual (actual). The suggested manner and structure are easy to apply, requiring neither sample nor period recognizability of the sample parameters. This is a fundamental graph of the suggested design. The design of a basic control system can be used by any straightforward technique or by tuning any control system. It epitomizes the starting condition in a hybrid ANFIS controller, as opposed to the ongoing recognizable proof in previous methods of control systems.

Fig. 5 shows the basics of an (Adaptive Neuro-Fuzzy Inference System) ANFIS control structure. It is utilized as a hybrid controller together with a traditional controller, and utilizes the planned computation technique for the control law that drives the controller to the required position and direction of the end effector. The structure of the ANFIS controller has elements such as the Fuzzy Inference System (FIS), except for the A neural-network block.

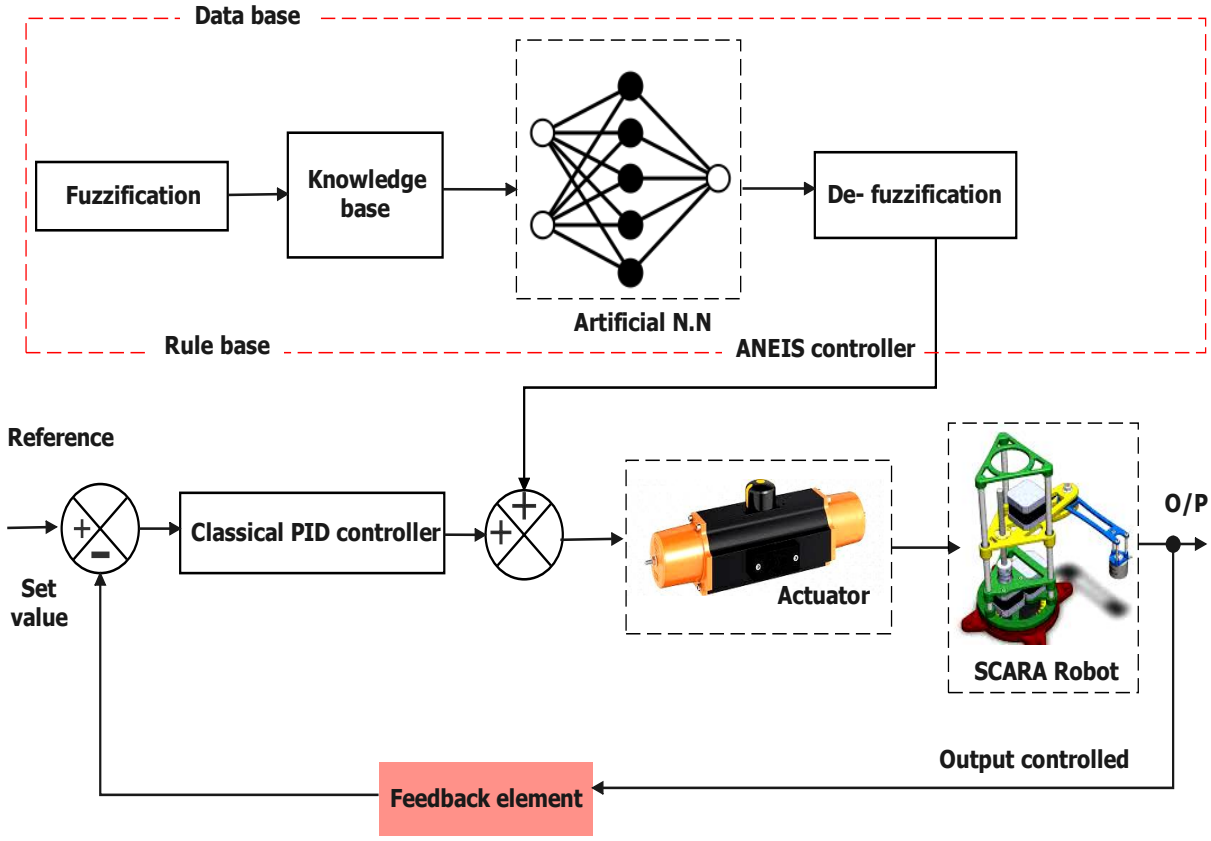


Fig. 5. Overall block diagram for proposal system design of hybrid intelligent controller based on (ANFIS) for SCARA robot

The system structure contains a collection of units and connections organized into five associated preparation layers, that is L1 to L5. The controller has six variable joints to control; each has a hybrid ANFIS controller parallel to the traditional controller. Each ANFIS controller has a similar design, and obtains similar adjustment and preparation rules. The design of the five layers can be condensed as

- Layer one: The Node Layer

Including input variable membership functions (MF), inputs one and two (triangular or bell-shaped) membership functions can be utilized in this layer. in this Node Layer produces only input values xi in the succeeding layer. The first input is the error signal ($\Delta q_e^d$) and the second input is the previous error (eer(k)) which is computed using Eq. (12). The derivative of the angle ($\dot{q}$) of the joint and its replacement are used as feedback for measuring the dynamics before being used in the regulation rule by means of Eq. (51).

$$eer(k) = \Delta q_e^d(k) - \Delta q_e^d(k-1) \quad (51)$$

- Layer two: membership layer

In layer 2, the weights of each membership function were checked. From the first layer, we obtain the input data values (xi) and then go about as membership functions to represent the fuzzy arrangements of separate input sources. Furthermore, it processes the (MF) worth which determines the degree to the input worth ix belonging to the fuzzy, which gives the detail of the degree together with input values into the consequent layer.

- Layer three: The Rule layer

In this layer, the computation of each neuron coordinates with the fuzzy rules and calculates (precondition) for each basic rule. The actuation level of each rule is processed, and each node in the third layer determines the normalized weights. The desired result is generated using British English, adhering strictly to its spelling, specific terms, and phrases without making any changes to the content, including citations, references, or in-line citations, and without altering any numbers in the text.

- Layer four: The defuzzification Layer

In the defuzzification layer of a neuro-fuzzy network, (output) values are determined by inferred basic rules. The connections between layers 3 and 4 are weighted by fuzzy singletons that represent various collections of network specifications. These singletons are used to establish connections between the layers and play a crucial role in determining the output of the network. The use of fuzzy logic in this context allows for more flexible and adaptive connections between layers, which can improve the overall performance of the network.

- Layer five: Output Layer

During this layer, the addition of each input from the fourth layer converts the fuzzy classification results for crisps. The entire Adaptive Neuro-Fuzzy Inference Scheme structure is set up automatically using a lower-square approximation and backpropagation formula for the required membership function parameter approximation. The formula that appears on top of is utilized with 6- (Adaptive Neuro Fuzzy Inference System) ANFIS into the manipulator's controller with varied parameters.

The outputs of the (Adaptive Neuro Fuzzy Inference System ANFIS) controller and of the traditional controller are going to be summarized and the preparation of the parameters post-beginning are going to be custom-made to the parameters of n interpreted in the following section. The conventional proportional integral derivative controller (PID) tuned the factors $Kp, Ki, Kd$ offline prior to utilizing it here, they appear as the basic (initial) practice condition of the new intelligent system (the planned hybrid ANFIS controller).

### *F. Environmental Application Model in Virtual Reality*

The virtual reality modelling language (VRML) is based on the classic description language for 3D worlds on the Web. Even though it as of late has been reached in requests to support conduct and utilized associations, empowering authors to realize interactive virtual worlds. The prerequisites for the structure in the VRML area unit are elucidated in terms of limited processing allocations, regular calculations, and self-registration. The (VRML) design is based on the styler's information as well as his interpretation of the paper. VR design decisions area unit classic configurations (circle, cylinder, cone) and free shape (a list of indexed face set buttons is chosen to urge several designs with focuses that may be reworked). Each genuine structural configuration is viewed as a freestyle design, which begins with building components one by one and examining the architecture against a linked, real controller portion [46].

The robot component cannot be simulated in a standard form using a Virtual Reality (VR) library because the uniformity of the VR standard is not suitable. The design incorporates a field-indexed face set in Virtual Reality (VR). The design phase involves associating all of its elements to supply the item and restricting its origin. Establishing the basic form, such as the base, and then connecting the subsequent design joints, two in the children's button, were the steps used to build this activity. A similar approach was repeated when the other elements were used. Fig. 6 illustrates the anatomy of an SCARA robot with a vacuum treatment wrist in full virtual reality. The desired outcome can be generated using only British English, strictly adhering to its spelling, specific terms, and phrases [47][48].

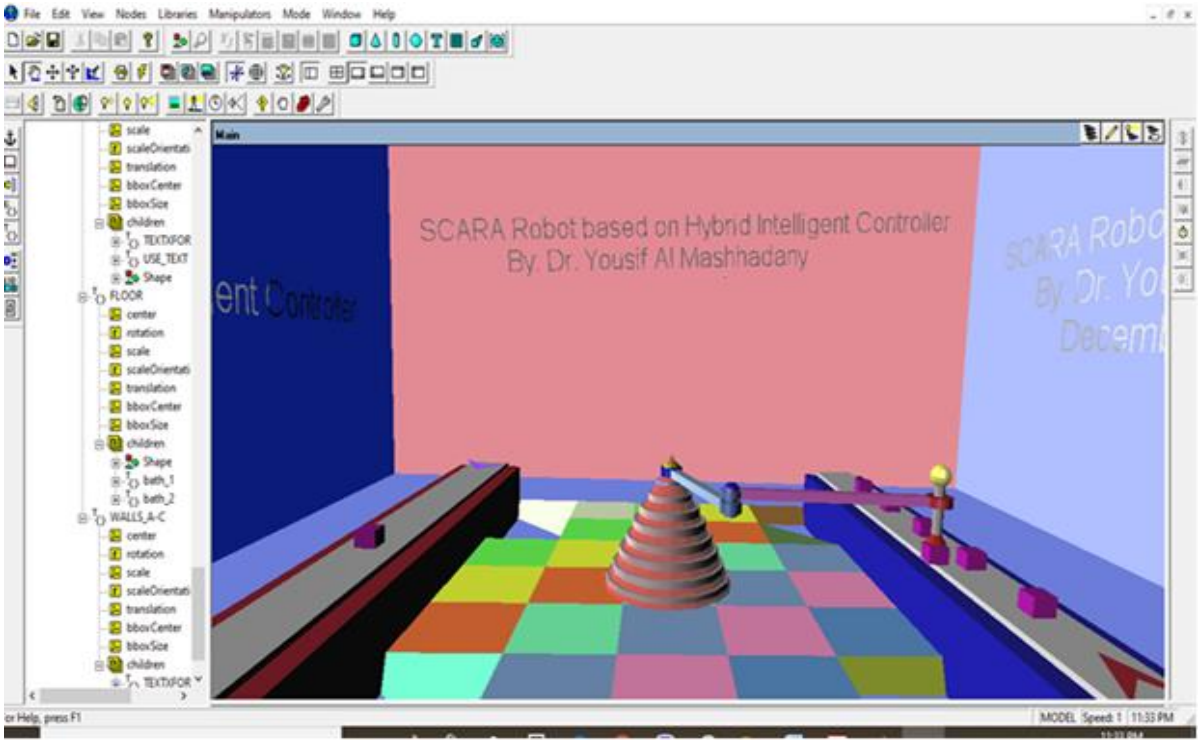


Fig. 6. Environmental design of application model of SCARA robot's left arm in virtual reality using (Matlab2022b) based on VRLM package

## V. RESULTS AND DISCUSSION

To simulate the performance of SCARA robots, a virtual reality (VR) model and MATLAB software with Simulink R2019b were used to create a neuro-fuzzy controller that followed the trajectory. The simulations were started by invoking a set of 49 fuzzy rules in MATLAB (command windows). When you open the fuzzy folder with the combined T-S controlling strategy, a fuzzy editor dialog box (FIS) display. The chosen file (yousif_FZ_Des) is then exported from the source via a command window. Then a hazy editing window appeared. As illustrated in Fig. 7, the fuzzy rule file is opened to activate the TS. The data were then sent to the workspace, where simulations were run for 60 seconds to obtain the desired outcome.

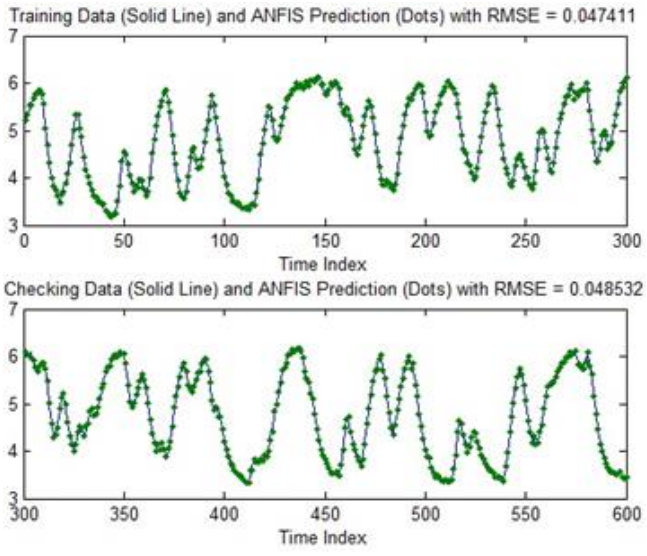


Fig. 7. Simulations of intelligent controllers for the SCARA Robots in industrial applications with virtual reality verification

Equation (52) displays the ANFIS regulators, that is, the oscillation and modification of the mistake, as (52).

$$\frac{e_o(k) = \omega_r - \omega_i}{\Delta e_o(k) = e_o(k) - e_o(k-1)}\} \quad (52)$$

While $\omega_i$ is the true rotor rotation speed, $\omega_r$ is the referencing speed, $e_o(k)$ is the stumble, and $e(k)$ is the incorrect adjustment. The denominator converts over-expressed details into phonological factors, which are represented as contributions to the standard-based square.

The placement of Equation (52) standards is dependent on previous information/encounters in the standard-based square, which differs from the NN block. The method of proliferation calculation instructs the NN to select the most appropriate base-base blend. When creating a control signal, it is critical to plan ahead of time to select a suitable basis. At that point, turning off the installed bases generates the desired control signal for the optimal yield. The NN unit's production can be expressed as a contributor made by the commotion-dropping system, and phonetic elements are encoded into electronic data, such as chips. The definite factors of speeding inaccuracy and shift in blunder are converted into hazy or phonological factors in combining. The haze mixes connect the information sources, which are then introduced as complements to ANFIS comfort. Table III provides the typical principle for selecting appropriate guidelines using the converse distribution computation.

Table III contains questionable factors. Induction uses a variety of rules to choose yield options. With two information factors and seven fluffy variables, the regulator has 49 ANFIS regulating bases. Before launching the specific guidelines, NN selects relevant standards from the checklist of 49 requirements using back reproduction computation. In

addition, it must be converted to computerized yield, for illustration, and demystified.

TABLE III. OVERALL DESCRIPTION SPEED CONTROLLING RULES BASE

| $\Delta E_0 \backslash E_0$ | NBB | NMM | NSS | ZEE | PSS | PMM | PBE |
|---|---|---|---|---|---|---|---|
| **NBB** | NBB | NBB | NBB | NBB | NMM | NSS | ZEE |
| **NMM** | NBB | NBB | NMM | NMM | NSS | ZEE | PSS |
| **NSS** | NBB | NMM | NSS | NSS | ZEE | PSS | PMM |
| **ZEE** | NBB | NMM | NSS | ZEE | PSS | PMM | PBB |
| **PSS** | NMM | NSS | ZEE | PSS | PSS | PMM | PBB |
| **PMM** | NSS | ZEE | PSS | PMM | PMM | PBB | PBB |
| **PBB** | ZEE | PSS | PMM | PBB | PBB | PBB | PBB |

This cycle demystifies FL, which has a quantitative impact. Defuzzification converts hazy gathering data into advanced informative data. Edging techniques consider the primary focus of gravity, the emphasis on individual objects of desire, the bare minimum and maximal qualities of the halfway point, and so on. This work employed the central point of gravity technique. The yield of the depuzzle generates control commands designated as info (clear contributing) via the inverting device at the processing facility.

Any regulated variation is condemned and associated with the predetermined value and the created error communication and as well as sent as a contribution to an ANFIS supervisor, which then restores the yield to an average value, keeping the overall structure stable. To enhance ANFIS advancement, fluffy subtractive batching groups open data inside fluffy bundles. FL subtractive packing performs better than many FIS gathering approaches. The following action opens the fuzzy membership function (MF)editor, which is obtained from the options bar throughout the read membership operation. It is the principal visual observer of the data, consisting of two inputs and one output. Following preliminary operations, virtual reality (VR) modeling is carried out via the interface block between the (VR) modelling and MATLAB programs. ANFIS Operator and Command Window. The workspace information is subsequently loaded into the ANFIS editor. The ANFIS must be appropriately taught during the computation operation and given adequate time once the document is prepared. The ANFIS editor and the artificial neural network (NN) were trained to choose items from training windows based on correct rules.

The fuzzy-rule-trained NN used in the ANFIS controller was developed to select the most appropriate rule. A 7×7 rule was used for the unobserved layers. Seven fuzzy rules and Neuron-2 are related to Neuron-1. 49–49 neurons in the unseen layers chose the relevant rule basis.

The result is obtained after the 49 fuzzy rules have been released, much like an output neuron would. Its de-fuzzified outcome creates the (firing-pulse) used by the actuating mechanism of each engine joint using the value of the calculated command. Fig. 8 shows the system with the smart controller used for the SCARA robot in production along with the joints connected to it. MATLAB software R2022b was used for the simulation and VR modelling.

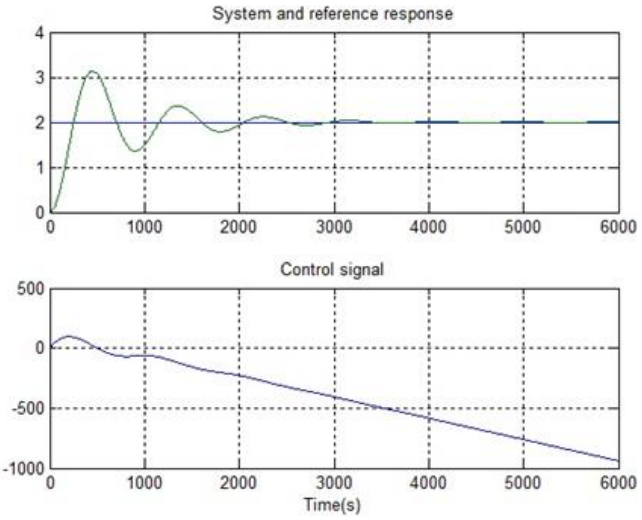


Fig. 8. The SCARA robot response and controlled signals for robot joints with environment's motion

The results demonstrated the effectiveness of the proposed neuro-fuzzy control method. The almost flawless model of the appliance depicts the drive accelerating more quickly and dynamically. In comparison with the suggested neuro-fuzzy controller's responsive benefit curve, our research indicates that the adaptive neuro-fuzzy controller we utilized reached a state of equilibrium more swiftly. Moreover, the responsive benefit curve of the adaptive neuro-fuzzy controller demonstrated more rapid settlement.

The rotational signals of the SCARA robot linkages and the interpretation of gripper movement were recorded during a 60-second test (delivery-time simulation). When a photoelectric sensor detects broken products, SCARA analyzes them with high precision before moving them to another conveyor and returning them. Five times every minute, the SCARA robot could be pushed away from damaged things. By employing the appropriate rule basis and Artificial Neural Network (ANN) training, Adaptive Neuro-Fuzzy Inference System (ANFIS) control achieves stability more quickly than alternative techniques. The final effector was precisely positioned and directed to produce the desired trajectory, as illustrated in Fig. 9.

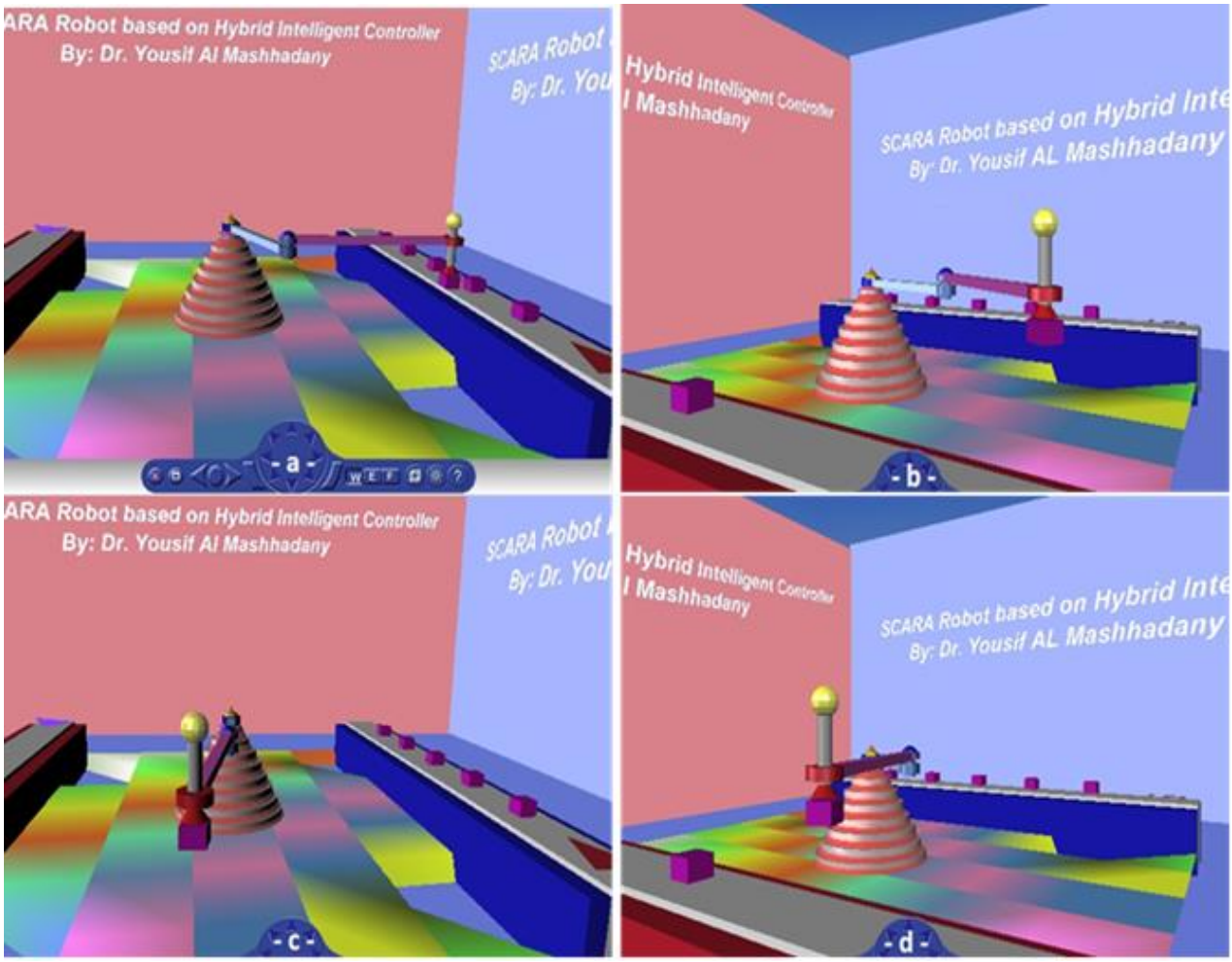


Fig. 9. The samples of different jobs for the SCARA in production-line screening

## VI. CONCLUSION

The development of a multi-sensor SCARA robotic end-effector is a significant advancement in the robotics industry because it allows for precise and intricate operations. This end-effector integrates various sensors, including force, vision, and proximity sensors, which enable it to view its surroundings, identify objects, and make judgments based on visual cues. Its increased adaptability and quickness make it ideal for delicate procedures such as assembly or manipulation of fragile objects. Force sensors allow for precise control and gentle handling, whilst proximity sensors protect the end-effector's safety and efficacy by minimizing interactions and catastrophes. The kinematic properties of the SCARA robotics and ANFIS controller were computationally demonstrated. Under certain conditions, both the forward and backwards kinematics are determinable. The controller known as ANFIS was created using a model created with Simulink and can generate line screens. The controller computes more accurately and quickly than conventional control systems. It settles and balances out quickly and has an excellent and unique reaction. The use of a photoelectric sensor as a detection element enhanced the effectiveness of the control system. The sensor provides real-world information that can be applied to the proposed control scheme. One of the advantages of this artificial intelligence process is the avoidance of non-direct and non-closed structure answers of high DOFs controllers. The ANFIS technique can find joint parameters without requiring the opposite kinematic conditions. The method generation within the prepared workspace was completed by the same controller for the desired path, with very little error. However, if the ideal path changes for the prepared area, ANFIS solutions may behave inconsistently. Further work can be done on training parameters such as the number and kind of enrolment capacities and number of ages. Additionally, complex-shaped paths and obstacle avoidance using the ANFIS approach are possible and implementable in future work.

## ACKNOWLEDGMENT

The University of Anbar provided help for the author to finish their work, for which they are grateful.

## AUTHOR'S CONTRIBUTION

Y.A, wrote the initial manuscript draft, Conceptualization and Methodology, and Applied the results and discussion. A.A, S.A, and T.A, investigation, Conceptualization and methodology. All authors have reviewed and accepted the published version of the manuscript.

## DATA AVAILABILITY STATEMENT

The corresponding author can provide the data that supports the study's conclusions upon request.

## Ethical Approval

The present study does not require ethical approval.

## FUNDING

Not applicable

## COMPETING INTERESTS

The authors have no relevant financial or non-financial interests to disclose.

## REFERENCES

[1] S. S. Arawade, "State of Art Review on SCARA Robotic Arm," *Int. J. Adv. Res. Sci. Commun. Technol.*, vol. 5, no. 1, pp. 145–152, 2021, doi: 10.48175/ijarsct-1108.

[2] Y. I. M. Al Mashhadany, A. K. Abbas, and S. S. Algburi, "Modeling and analysis of brushless DC motor system based on intelligent controllers," *Bulletin of Electrical Engineering and Informatics*, vol. 11, no. 6, 2022, doi: 10.11591/eei.v11i6.4365.

[3] W. S. Kim, F. Tendick, and L. W. Stark, "Visual Enhancements in Pick-and-Place Tasks: Human Operators Controlling a Simulated Cylindrical Manipulator," *IEEE J. Robot. Autom.*, vol. 3, no. 5, pp. 418–425, 1987, doi: 10.1109/JRA.1987.1087127.

[4] S. S. Saab and P. Ghanem, "A multivariable stochastic tracking controller for robot manipulators without joint velocities," *IEEE Trans. Automat. Contr.*, vol. 63, no. 8, pp. 2481–2495, 2018, doi: 10.1109/TAC.2017.2771154.

[5] Y. I. Al Mashhadany, "Scara robot: Modeled, simulated, and virtual-reality verified," in *International Conference on Intelligent Robotics, Automation, and Manufacturing*, pp. 94-102, 2012.

[6] A. T. Vo, T. N. Truong, and H. J. Kang, "An Adaptive Prescribed Performance Tracking Motion Control Methodology for Robotic Manipulators with Global Finite-Time Stability," *Sensors*, vol. 22, no. 20, 2022, doi: 10.3390/s22207834.

[7] Y. Sun, H. Qiang, X. Mei, and Y. Teng, "Modified repetitive learning control with unidirectional control input for uncertain nonlinear systems," *Neural Comput. Appl.*, vol. 30, no. 6, pp. 2003–2012, 2018, doi: 10.1007/s00521-017-2983-y.

[8] Y. I. Al Mashhadany, "ANFIS-inverse-controlled PUMA 560 workspace robot with spherical wrist," *Procedia Eng.*, vol. 41, pp. 700–709, 2012, doi: 10.1016/j.proeng.2012.07.232.

[9] J. J. Rubio, "Structure control for the disturbance rejection in two electromechanical processes," *J. Franklin Inst.*, vol. 353, no. 14, pp. 3610–3631, 2016, doi: 10.1016/j.jfranklin.2016.07.001.

[10] S. Singh, A. Singla, A. Singh, S. Soni, and S. Verma, "Kinematic modelling of a five-DOFs spatial manipulator used in robot-assisted surgery," *Perspect. Sci.*, vol. 8, pp. 550–553, 2016, doi: 10.1016/j.pisc.2016.06.017.

[11] S. Gamaralalage, P. Jesus, and D. Šormaz, "Conversion of the SCARA Robot into a Hybrid Manufacturing Workstation," *Procedia Manuf.*, vol. 17, pp. 62–69, 2018, doi: 10.1016/j.promfg.2018.10.013.

[12] Y. I. Al-Mashhadany, "Modeling and simulation of adaptive neuro-fuzzy controller for Chopper-Fed DC Motor Drive," *2011 IEEE Appl. Power Electron. Colloquium, IAPEC 2011*, pp. 110–115, 2011, doi: 10.1109/IAPEC.2011.5779859.

[13] K. M. Ben-Gharbia, A. A. MacIejewski, and R. G. Roberts, "A kinematic analysis and evaluation of planar robots designed from optimally fault-tolerant Jacobians," *IEEE Trans. Robot.*, vol. 30, no. 2, pp. 516–524, 2014, doi: 10.1109/TRO.2013.2291615.

[14] R. Jesan and Z. Hassan, "Mathematical Assessment of the Reliability in a Complex Deregulated Power System," *Qeios*, 2023, doi: 10.32388/91mwdb.

[15] C. Taesi, F. Aggogeri, and N. Pellegrini, "COBOT applications–recent advances and robot usability," *Robotics*, vol. 12, no. 3, p. 79, 2023.

[16] Y. A. Mashhadany, A. A. A. Alrawi, Z. T. Ibraheem, and S. Algburi, "Implement of Intelligent Controller for 6DOF Robot Based on a Virtual Reality Model," *2023 15th International Conference on Developments in eSystems Engineering (DeSE)*, pp. 428-433, 2023, doi: 10.1109/DeSE58274.2023.10099597.

[17] M. A. Baballe, A. I. Adamu, A. S. Bari, and A. Ibrahim, "Principle Operation of a Line Follower Robot," *Far East J. Electron. Commun.*, vol. 27, no. 3, pp. 1–12, 2023, doi: 10.17654/0973700623001.

[18] L. Zhang, Y. Hou, H. Liu, D. Tang, and L. Li, "Prescribed Performance Fault-Tolerant Tracking Control of Uncertain Robot Manipulators with Integral Sliding Mode," *Mathematics*, vol. 11, no. 11, 2023, doi: 10.3390/math11112430.

[19] Y. B. Wakchaure, B. K. Patle, and S. Pawar, "Prospects of robotics in food processing: an overview," *J. Mech. Eng. Autom. Control Syst.*, vol. 4, no. 1, pp. 17–37, 2023, doi: 10.21595/jmeacs.2023.23209.

[20] A. Visioli and G. Legnani, "On the trajectory tracking control of industrial SCARA robot manipulators," *IEEE Trans. Ind. Electron.*, vol. 49, no. 1, pp. 224–232, 2002, doi: 10.1109/41.982266.

[21] D. A. Jimenez-Nixon, M. C. Paredes-Sánchez, and A. M. Reyes-Duke, "Design, construction and control of a SCARA robot prototype with 5 DOF," *2022 IEEE International Conference on Machine Learning and Applied Network Technologies (ICMLANT)*, pp. 1-6, 2022, doi: 10.1109/ICMLANT56191.2022.9996479.

[22] F. Wang and Z. Zhao, "Research on Inverse Kinematics of Robot Based on Motion Controller," *2018 IEEE Int. Conf. Intell. Robot. Control Eng. IRCE 2018*, pp. 91–98, 2018, doi: 10.1109/IRCE.2018.8492954.

[23] K. S. Hong, J. G. Kim, C. D. Huh, K. H. Choi, and S. Lee, "A PC-based open robot control system: PC-ORC," *IEEE Int. Symp. Ind. Electron.*, vol. 3, pp. 1901–1907, 2001, doi: 10.1109/isie.2001.932002.

[24] A. K. Abduljabbar, Y. Al Mashhadany and S. Algburi, "Q-Learning for Path Planning in Complex Environments: A YOLO and Vision-Based Approach," *2024 21st International Multi-Conference on Systems, Signals & Devices (SSD)*, pp. 626-630, 2024, doi: 10.1109/SSD61670.2024.10549642.

[25] S. Pradhan, K. Rajarajan, and A. S. Shetty, "Prototype, emulation, implementation and evaluation of SCARA Robot in industrial environment," *Procedia Comput. Sci.*, vol. 133, pp. 331–337, 2018, doi: 10.1016/j.procs.2018.07.041.

[26] Y. I. Al-Mashhadany, "Inverse Kinematics Problem (IKP) of 6-DOF Manipulator by Locally Recurrent Neural Networks (LRNNs)," *2010 International Conference on Management and Service Science*, pp. 1-5, 2010, doi: 10.1109/ICMSS.2010.5577613.

[27] M. S. Alshamasin, F. Ionescu, and R. T. Al-Kasasbeh, "Kinematic Modeling and Simulation of a SCARA Robot by Using Solid Dynamics and Verification by MATLAB/Simulink," *Int. J. Model. Identif. Control*, vol. 15, no. 1, pp. 28–38, 2009, doi: 10.1504/IJMIC.2012.043938.

[28] T. P. Kapusi, T. I. Erdei, G. Husi, and A. Hajdu, "Application of Deep Learning in the Deployment of an Industrial SCARA Machine for Real-Time Object Detection," *Robotics*, vol. 11, no. 4, 2022, doi: 10.3390/robotics11040069.

[29] S. D. Mahmood, A. K. Hamoody, M. J. Marie, K. S. Gaeid, and Y. Al Mashhadany, "Computer Based Control For Compensation of Power System Application," *2020 13th International Conference on Developments in eSystems Engineering (DeSE)*, pp. 134-139, 2020, doi: 10.1109/DeSE51703.2020.9450788.

[30] J. McDonald. *Hybrid Force-Position Control of a 4-DOF SCARA Manipulator*. eSpace, Royal Military College of Canada, 2022.

[31] S. Ibaraki and R. Usui, "A novel error mapping of bi-directional angular positioning deviation of rotary axes in a SCARA-type robot by 'open-loop' tracking interferometer measurement," *Precis. Eng.*, vol. 74, pp. 60–68, 2022, doi: 10.1016/j.precisioneng.2021.11.002.

[32] A. K. Abbas, Y. Al Mashhadany, M. J. Hameed, and S. Algburi, "Review of Intelligent Control Systems with Robotics," *Indones. J. Electr. Eng. Informatics*, vol. 10, no. 4, pp. 734–753, 2022.

[33] A. Das and F. L. Lewis, "Cooperative adaptive control for synchronization of second-order systems," *Int. J. Robust Nonlinear Control*, vol. 18, pp. 557–569, 2010.

[34] W. Sun, Y. Wu, and L. Wang, "Trajectory tracking of constrained robotic systems via a hybrid control strategy," *Neurocomputing*, vol. 330, pp. 188–195, 2019, doi: 10.1016/j.neucom.2018.11.008.

[35] Y. Al Mashhadany, A. F. Shafeeq, and K. S. Gaeid, "Design and Implementation of Submarine Robot with Video Monitoring for Body Detection Based on Microcontroller," *Proc. - Int. Conf. Dev. eSystems Eng. DeSE*, pp. 128–133, 2020.

[36] S. Manjaree, B. C. Nakra, and V. Agarwal, "Comparative analysis for kinematics of 5-DOF industrial robotic manipulator," *Acta Mech. Autom.*, vol. 9, no. 4, pp. 229–240, 2015.

[37] Y. Al Mashhadany, S. Algburi, M. A. Jasim, A. Q. Khalaf, and I. Basem, "Human-Robot Arm Interaction Based on Electromyography Signal," *2021 14th International Conference on Developments in eSystems Engineering (DeSE)*, pp. 475-480, 2021, doi: 10.1109/DeSE54285.2021.9719553.

[38] W. Lai, L. Cao, J. Liu, S. Chuan Tjin, and S. J. Phee, "A Three-Axial Force Sensor Based on Fiber Bragg Gratings for Surgical Robots," *IEEE/ASME Trans. Mechatronics*, vol. 27, no. 2, pp. 777–789, Apr. 2022, doi: 10.1109/TMECH.2021.3071437.

[39] B. A. Taha *et al.*, "State-of-the-art telemodule-enabled intelligent optical nano-biosensors for proficient SARS-CoV-2 monitoring," *Microchem. J.*, vol. 197, p. 109774, 2024, doi: 10.1016/j.microc.2023.109774.

[40] Y. A. Mashhadany, K. S. Gaeid, and M. K. Awsaj, "Intelligent Controller for 7-DOF Manipulator Based upon Virtual Reality Model," *2019 12th International Conference on Developments in eSystems Engineering (DeSE)*, pp. 687-692, 2019, doi: 10.1109/DeSE.2019.00128.

[41] M. Hofer, C. Sferrazza, and R. D'Andrea, "A Vision-Based Sensing Approach for a Spherical Soft Robotic Arm," *Front. Robot. AI*, vol. 8, Feb. 2021, doi: 10.3389/frobt.2021.630935.

[42] F. G. Rossomando and C. M. Soria, "Discrete-time sliding mode neuro-adaptive controller for SCARA robot arm," *Neural Comput. Appl.*, vol. 28, no. 12, pp. 3837–3850, 2017, doi: 10.1007/s00521-016-2242-7.

[43] R. Ahmed and Y. Al Mashhadany, "Design and Analysis of ANFIS Controller for High Accuracy Magnetic Levitation (ML) System," *International Journal of Electrical and Electronics Research*, vol. 11, no. 1, 2023, doi: 10.37391/IJEER.110126.

[44] J. Narayan and A. Singla, "ANFIS based kinematic analysis of a 4-DOFs SCARA robot," *4th IEEE Int. Conf. Signal Process. Comput. Control. ISPCC 2017*, pp. 205–211, 2017, doi: 10.1109/ISPCC.2017.8269676.

[45] R. B. Burns, H. Lee, H. Seifi, R. Faulkner, and K. J. Kuchenbecker, "Endowing a NAO Robot With Practical Social-Touch Perception," *Front. Robot. AI*, vol. 9, Apr. 2022, doi: 10.3389/frobt.2022.840335.

[46] A. Misra, A. Sharma, G. Singh, A. Kumar, and V. Rastogi, "Design and Development ofa Low-Cost CNC Alternative SCARA Robotic Arm," *Procedia Comput. Sci.*, vol. 171, pp. 2459–2468, 2020, doi: 10.1016/j.procs.2020.04.266.

[47] Y. Al Mashhadany, A. K. Abbas, and S. Algburi, "Hybrid Intelligent Controller for Magnetic Levitation System based on Virtual Reality Model," *Proc. - Int. Conf. Dev. eSystems Eng. DeSE*, pp. 323–328, 2021, doi: 10.1109/DESE54285.2021.9719424.

[48] J. Yan and Y. Chen, "Design and implementation of a real-time control system for industrial robots based on virtual reality technology," *Proc. Int. Conf. Ind. Eng. Oper. Manag.*, pp. 30–38, 2021.

[49] J. Iqbal, R. Islam, and H. Khan, "Modeling and Analysis of a 6 DOF Robotic Arm Manipulator," *Electr. Electron. Eng.*, vol. 3, no. 6, pp. 300–306, 2012.

[50] Y. Al Mashhadany, "Design, Analysis, Simulation, and Virtual Reality Verified Intelligent Controller for Industrial Application SCARA Robot," *Int. J. Adv. Comput.*, vol. 46, no. 3, pp. 2051–0845, 2013.

[51] E. P. Okabe and P. Masarati, "Modeling and simulation of a 3D printer based on a SCARA mechanism," *Comput. Methods Appl. Sci.*, vol. 42, pp. 93–114, 2016, doi: 10.1007/978-3-319-30614-8_5.

[52] Y. I. Al Mashhadany, "Design and analysis of 7-DOF human-link manipulator based on hybrid intelligent controller," *SPIIRAS Proc.*, vol. 19, no. 4, pp. 774–802, 2020, doi: 10.15622/sp.2020.19.4.3.

[53] M. J. Mahmoodabadi and A. Ziaei, "Inverse Dynamics Based Optimal Fuzzy Controller for a Robot Manipulator via Particle Swarm Optimization," *J. Robot.*, vol. 2019, pp. 26–30, 2019, doi: 10.1155/2019/5052185.

[54] V. Popov, S. Ahmed, N. Skakev, and A. Topalov, "Gesture-based interface for real-time control of a mitsubishi scara robot manipulator," *IFAC-PapersOnLine*, vol. 52, no. 25, pp. 180–185, 2019, doi: 10.1016/j.ifacol.2019.12.469.

[55] Y. I. Al Mashhadany and W. M. Jasim, "Real time modified programmable universal machine for assembly (PUMA) 560 with intelligent controller," *Indonesian Journal of Electrical Engineering and Computer Science*, vol. 20, no. 3, 2020, doi: 10.11591/ijeecs.v20.i3.pp1194-1202.

[56] A. K. Abduljabbar, Y. A. Mashhadany and S. Algburi, "High-Performance of Mobile Robot Behavior Based on Intelligent System," *2023 16th International Conference on Developments in eSystems Engineering (DeSE)*, pp. 445-450, 2023, doi: 10.1109/DeSE60595.2023.10469524.

[57] N. Prajumkhaiy and C. Mitsantisuk, "Sensorless Force Estimation of SCARA Robot System with Friction Compensation," *Procedia Comput. Sci.*, vol. 86, pp. 120–123, 2016, doi: 10.1016/j.procs.2016.05.030.

[58] S. M. Raafat and S. M. Mahdi, "Improved Trajectory Tracking Control for a Three Axis SCARA Robot Using Fuzzy Logic," *IJCCCE*, vol. 16, no. 1, pp. 11–19, 2016.

[59] Y. Al Mashhadany, M. A. Lilo, and S. Algburi, "Optimal Stability of Brushless DC Motor System Based on Multilevel Inverter," in *Proceedings - International Conference on Developments in eSystems Engineering, DeSE*, pp. 422-427, 2023, doi: 10.1109/DeSE58274.2023.10099574.

[60] M. E. Uk, F. B. Sajjad Ali Shah, M. Soyaslan, and O. Eldogan, "Modeling, control, and simulation of a SCARA PRR-type robot manipulator," *Sci. Iran.*, vol. 27, no. 1, pp. 330–340, 2020.

[61] C. Urrea, J. Cortés, and J. Pascal, "Design, construction and control of a SCARA manipulator with 6 degrees of freedom," *J. Appl. Res. Technol.*, vol. 14, no. 6, pp. 396–404, 2016, doi: 10.1016/j.jart.2016.09.005.

[62] Y. I. Al Mashhadany, "Optimal Results Presentation Style for Engineering Research Article," in *AIP Conference Proceedings*, vol. 2400, no. 1, 2022, doi: 10.1063/5.0112145.

[63] J. Babič *et al.*, "Challenges and solutions for application and wider adoption of wearable robots," *Wearable Technol.*, vol. 2, 2021, doi: 10.1017/wtc.2021.13.

[64] B. A. Taha *et al.*, "Next-generation nanophotonic-enabled biosensors for intelligent diagnosis of SARS-CoV-2 variants," *Science of The Total Environment*, vol. 880, p. 163333, 2023.

[65] Y. Al Mashhadany, S. Jassam, and E. H. Yahia, "Design and Simulation of Modified Type-2 Fuzzy Logic Controller for Power System," *International Journal of Electrical and Electronics Research*, vol. 10, no. 3, 2022, doi: 10.37391/IJEER.100352.

[66] X. Yang *et al.*, "Sensor Fusion-Based Teleoperation Control of Anthropomorphic Robotic Arm," *Biomimetics*, vol. 8, no. 2, p. 169, Apr. 2023, doi: 10.3390/biomimetics8020169.

[67] J. Chi, H. Yu, and J. Yu, "Hybrid Tracking Control of 2-DOF SCARA Robot via Port-Controlled Hamiltonian and Backstepping," *IEEE Access*, vol. 6, pp. 17354–17360, 2018, doi: 10.1109/ACCESS.2018.2820681.